Analysis of the influence of external biasing on Texas Helimak turbulence

D. L. Toufen,[1,2,a)] Z. O. Guimarães-Filho,[1] I. L. Caldas,[1] J. D. Szezech,[3] S. Lopes,[4] R. L. Viana,[4] and K. W. Gentle[5]

[1]*Institute of Physics, University of São Paulo, C.P. 66318, 05315-970 São Paulo, São Paulo, Brazil*
[2]*Federal Institute of Education, Science and Technology of São Paulo—IFSP, 07115-000 Guarulhos, São Paulo, Brazil*
[3]*Department of Physics, State University of Ponta Grossa, 84030-900 Paraná, Brazil*
[4]*Department of Physics, Federal University of Paraná, 81531-990 Curitiba, Paraná, Brazil*
[5]*Department of Physics and Institute for Fusion Studies, The University of Texas at Austin, Austin, Texas 78712, USA*

We analyze alterations on the electrostatic turbulence in experiments with imposed bias to control the plasma radial electric field in Texas Helimak (K. W. Gentle and H. He, Plasma Sci. Technol. **10**, 284 (2008)), a toroidal plasma device with a one-dimensional equilibrium, magnetic curvature, and shear. Comparing discharges from different biased potentials, we identify, in a roughly uniform gradient region, a continuous variation from low turbulence level and narrower frequency spectra, for negative bias, to high turbulence level and broadband spectra for positive bias. Overall, we distinguish two kinds of perturbed turbulence, classified according to their intensity, spectral, statistical, and recurrence properties. When the bias is positive, the turbulence shows enhanced and broadband spectra with non Gaussian probability distribution functions having noticeable long tails (extreme events) similar to the turbulence in tokamak scrape-off layer. On the other hand, negative bias reduces the turbulence level and decreases the spectrum widths. Also for negative bias, we found large frequency widths whenever the coupling between drift waves and the sheared plasma flow is fast enough to allow the enhancement of sidebands modes. © *2013 American Institute of Physics*. [http://dx.doi.org/10.1063/1.4793732]

I. INTRODUCTION

Improvement of plasma confinement in toroidal devices, as tokamaks and stellarators, is limited by the electrostatic turbulence observed at the edge region.[1–4] In the last years, several works have investigated how to control plasma turbulence and improve the confinement by imposing an external electric potential that changes the radial electric field profile.[5–8] Although there has been reported progress, further investigations are necessary to complete the experimental description, of the reported turbulence alterations obtained by controlling the electric field, and to better understand the influence of the biased electric potential on the turbulence spectral properties.

In general, turbulent magnetically confined plasmas display broadband fluctuation power spectra[3] and the associated wave coupling interaction are considered essential for explaining this broadband power spectra observed in laboratory settings.[9,10] It has also been observed that the radial electric field inside the plasma modifies the nonlinear wave interactions.[3,11,12]

Complementary investigations of plasma turbulence and their spectral characteristics have been carried out in several simple magnetized devices. One experimental work, on a linear device, showed that drift waves may destabilize and generate a turbulent spectrum.[13] Another experimental investigation showed that turbulence developed in a toroidal magnetoplasma due to drift wave destabilization by a large magnetic confinement field.[14] Moreover, in a toroidal device

without plasma current, anomalous transport was associated to intermittent large coherent vertical structures.[15] In a toroidal magnetoplasma created by radio frequency waves, without plasma current, the development of temporal turbulence was attributed to the increase of the confinement toroidal magnetic field.[16] In the large plasma device (LAPD),[17,18] investigations in turbulence and turbulent particle transport were performed due the capability of this device to create a variable electric field on the radial direction.[19]

Recently, electrostatic turbulence has also been investigated in plasmas with flow and magnetic shear in helimaks.[15,20–23] In these toroidal devices, several experiments have been performed to study the role of electrostatic instabilities on the turbulence onset. The helimak is one of a class of basic plasma experiments with characteristics of fusion plasmas in a simple geometry. This basic plasma toroidal device has a sheared cylindrical slab that simplifies the turbulence description and provides results that can be used to understand plasma edge and the scrape-off layer transport in major fusion machines.[24] As the plasma of helimak is colder and less dense when compared with tokamaks, it is possible to use a large set of diagnostic probes. These characteristics make the helimak an interesting device to study the plasma flow shear influence on wave turbulence.[21,25]

In Texas Helimak, turbulence biasing control has been investigated and, in the biased region, states of greatly reduced turbulence have been achieved.[8,20] Comparison of the shearing rates with the turbulence amplitudes as a function of bias showed no relation between the shearing rate and turbulence reduction, contrary to expectations.[11] Data analyzes revealed features of instabilities in Texas Helimak.[17,25] Recently,

---

a)Electronic mail: dennis@if.usp.br.

we analyzed the turbulence induced transport in this device and found evidence that transport is much affected by wave particle resonances and shearless transport barrier.[26]

In this article, we analyze the turbulence changes due to alterations on the radial electric field profile, in the plasma region of Texas Helimak with roughly uniform equilibrium gradients, through an external voltage bias applied to a set of border plates. For normal operation, all plates are connected to the vacuum vessel ground. For biased operation, some plates are connected to a controlled bias voltage. By applying spectral, statistical, and recurrence analyses, we identify two different kinds of perturbed turbulence. Overall, for positive biasing, turbulence shows enhanced broadband spectra and non Gaussian PDF with extreme events. On the other hand, during negative biasing the turbulence level is reduced. In this case, the spectral width increases with the wave coupling. Moreover, large frequency widths occur for short growth rate of the sidebands associated to the recursively coupling between the drift waves and the zonal flow.

In Sec. II, we review the experimental set up. In Sec. III, we describe turbulence in Texas Helimak and in Sec. IV the influence of external biasing on turbulence. In Sec. V, we discuss the reported experimental features and, finally, in Sec. VI we comment our main conclusions.

II. EXPERIMENTAL SET UP

The experiments are performed at Texas Helimak,[20] a basic plasma toroidal device located at the University of Texas at Austin. In this machine, the combination between the toroidal and the small vertical field creates a helical magnetic field with curvature and shear as shown Fig. 1(a). Most of these magnetic field lines start and terminate into four sets of four plates located at 180° apart at the top and the bottom part of the machine. These plates are used as a support to the Langmuir probes and to apply external electric potentials (bias) to change the radial electric field profile. The Helimak geometry is well described by the sheared cylindrical slab[24] since the connection lengths are long enough to neglect the end effects. In the analyzed experiments, the dominant toroidal field is about 0.1 T, which, when combined with the weaker vertical field create magnetic field lines with ≅40 m of connection length at the middle of the machine (R = 1 m). The field lines are thus helices as shown in Fig. 1(a), spiraling from bottom to top.

Texas Helimak has a vacuum vessel with rectangular cross section of external radius $R_{external} = 1.6$ m, internal radius $R_{internal} = 0.6$ m, and height = 2 m. For the experiments analyzed in this work, Argon gas at 10^{-5} Torr was heated by electron cyclotron resonance heating with 6 kW of power inserted by a window located on the inner side of the vacuum vessel. The shot duration is up to 20 s and the plasma is in a steady state with stationary conditions during 10 s, the time interval considered for fluctuation analyzes described in this work.

The diagnostic system count with more than 700 Langmuir probes mounted at the four sets of bias plates. The analyzed data were taken by two digitizers, one recently implanted, with 96 channels and 500 kHz of sample rate, and another one with 64 channels and 7 kHz of sample rate.
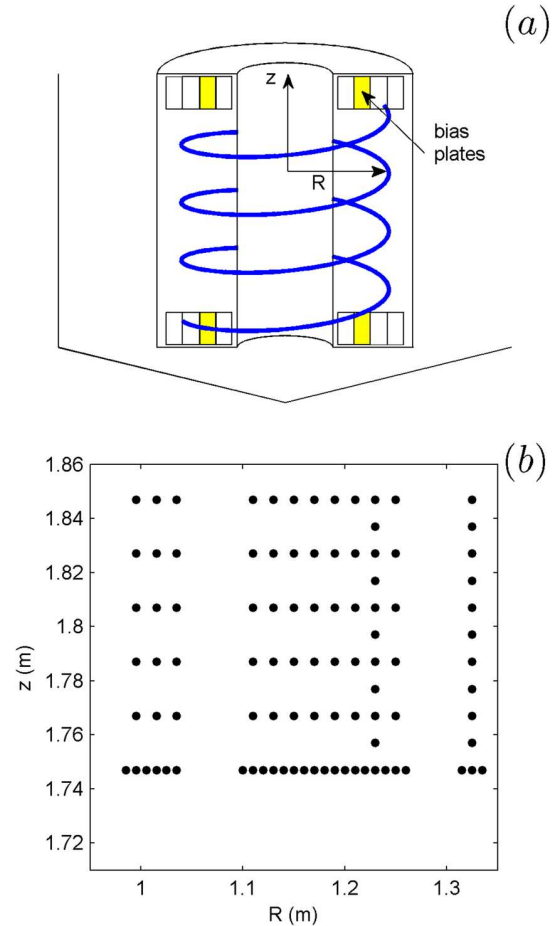

FIG. 1. (a) Cross section of Texas Helimak vacuum vessel showing the position of the four sets of bias plates (in yellow are those used for this work) and a sample of its helicoidally magnetic field lines. (b) Probe distribution, on the top plates, used to measure the fluctuating saturation current analyzed in this work.

The probe distribution shown in Fig. 1(b) was used to measure saturation current fluctuations analyzed in this work.

Figure 2 shows the mean density radial profile estimated from saturation current fluctuations and the mean floating
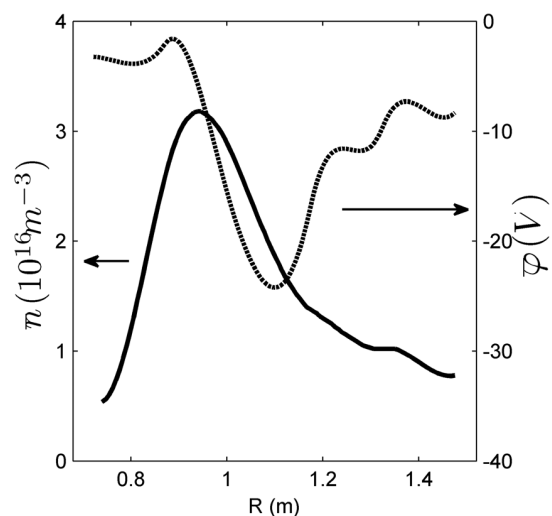

FIG. 2. Radial profiles of the equilibrium plasma density (in solid) estimated from current saturation and the equilibrium floating potential (in dashed).

potential radial profile. The density profile has a maximum at $R \cong 0.95$ m and decreases more smoothly on the external side of the peak, which corresponds to the low field side of the toroidal magnetic field. The mean floating potential radial profile presents a minimum at $R \cong 1.10$ m and a positive gradient in the analyzed radial region, $1.10\,\text{m} < R < 1.25\,\text{m}$. In this region, the density gradient is practically uniform and the electric field is much affected by the external bias imposed in the four bias plates positioned from $R = 0.86$ m to $R = 1.07$ m (marked in yellow in Fig. 1(a)).

III. TURBULENCE

To study plasma turbulence characteristics in Texas Helimak, we perform spectral analyses on the current saturation time series n(t) obtained for each probe in the configuration shown in Fig. 1(b). These signals were originally taken during the full shots of 22 s of duration but we only analyze the 9.7 s of stable plasma. As the series were acquired with recently implanted analog to digital converter with 500 kHz of sample rate, the considered time series have about 4.9×10^6 points.

For the spectral analysis, we perform a windowed FFT algorithm dividing each selected data time series into 194 series with 25×10^3 points each. Taken the $\phi_n(f)$ as the discrete Fourier transform of the n time signal at frequency f, the power density spectrum and the cross power spectrum are calculated by

$$S_{nn}(f) = \phi_n(f)\phi_n^*(f) \tag{1}$$

and

$$S_{nm}(f) = \phi_n(f)\phi_m^*(f), \tag{2}$$

where $\phi^*(f)$ represents the complex conjugate of $\phi(f)$.

With these spectra, we calculate the coherency spectrum, γ_{nm}, of the two different probes signals using the relation given by[9]

$$\gamma_{nm} = \frac{|\langle S_{nm} \rangle|}{(\langle S_{nn} \cdot S_{mm} \rangle)^{1/2}}. \tag{3}$$

Once the cross power spectrum can be written as

$$S_{nm}(f) = |S_{nm}(f)|e^{i\theta(f)}. \tag{4}$$

The vertical wave number spectrum, k(f), was calculated using the phase shift of the cross power spectrum of the signals of two probes placed in different vertical positions[9]

$$k(f) = \frac{\theta(f)}{\Delta d}. \tag{5}$$

The power density spectra for two probes at the same radial position, $R = 1.21$ m, and separated by $\Delta z = 4$ cm in the vertical direction are shown in Figs. 3(a) and 3(b). Both spectra show the same small peak, at $f \cong 100$ Hz, and power decay as a function of frequency. The coherency spectrum, Fig. 3(c), of these two probes present high and uniform coherency values for $f < 40$ kHz, due to plasma waves propagating in the
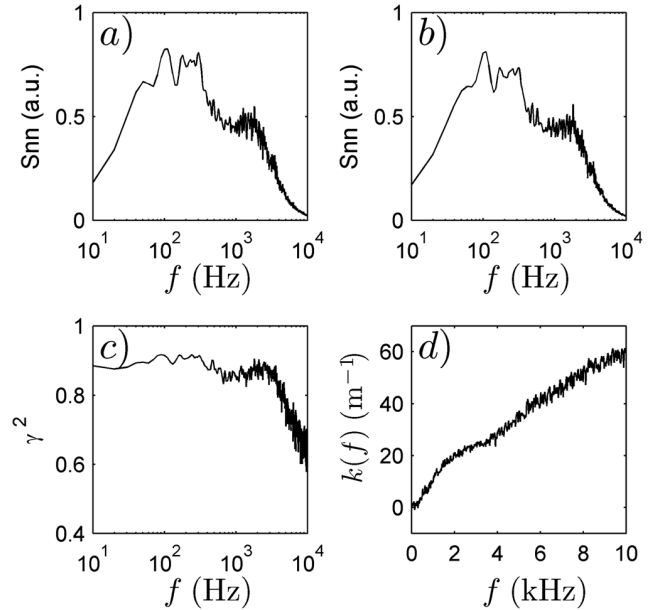

FIG. 3. Saturation current power spectra for two probes at the same radial position, $R = 1.21$ m, and different vertical positions: (a) $z = 1.75$ m and (b) $z = 1.77$ m. Frequency spectra of (c) coherency and (d) average wave number for these two probes. For this shot, the bias was grounded.

vertical direction. The average wave number presents a linear frequency dependence, Fig. 3(d), showing that all spectra have the same phase velocity.

To better characterize the dispersion relation, we can introduce the $S(k,f)$ spectrum, which can be estimated from two probe measurements as

$$S(k,f) = \sum_j \delta(k,k^j)\delta(f,f^j)|S^j_{nm}(f)|, \tag{6}$$

where $\delta(a,b)$ is the Kronecker delta and the index j represents each window of the Fourier transformer. Therefore, the local $S(k,f)$ spectrum is estimated as the bidimensional histogram of the amplitudes of the cross spectrum in terms of the wave number and frequency among several similar realizations. The $S(k,f)$ spectrum is observed in Fig. 4, in which we present in color scale the obtained signal power as a function of its frequency and wave number. This spectrum shows an almost linear relation between the wave numbers and frequencies with a similar dispersion for all measured frequencies, including the low frequency peak, indicating that the dominant waves propagate in the vertical direction with similar phase velocity.

Turbulence characteristics change with the radial position but are expected to be independent of the vertical position. To verify this dependence, we present in Fig. 5(a) the power spectrum width values, Δf, in color scale, obtained for probes placed in different positions whose radial and vertical coordinates, R and z, are indicated in the figure. The Δf is estimated by sorting the channels values of the power spectrum in descending order and then computing the number of channels that needs to be summed in order to reach half of the total spectral power. Figure 5(a) shows that the power spectrum width becomes broader with
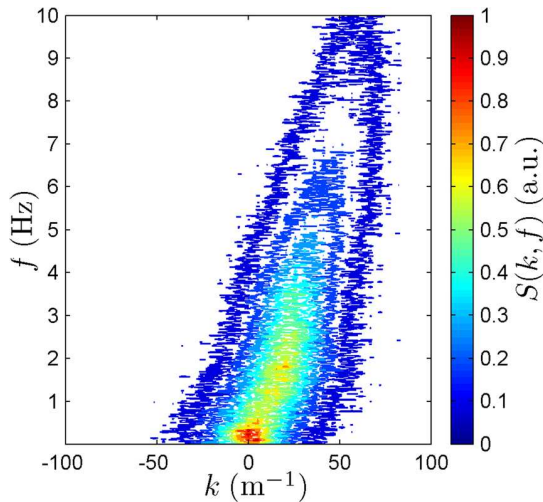
FIG. 4. Saturation current $S(k,f)$ spectrum for the probes (same of Fig. 3) at the radial position R = 1.21 m, and different vertical positions z = 1.75 m and z = 1.77 m. In this shot, the bias was grounded.

increasing R and is approximately independent of z. As the power spectrum width basically does not depend on the vertical coordinate, we calculate the mean value of the Δf on the z direction and the result is show in Fig. 5(b). The uncertainties are estimated by the standard deviation for the vertical set of values.
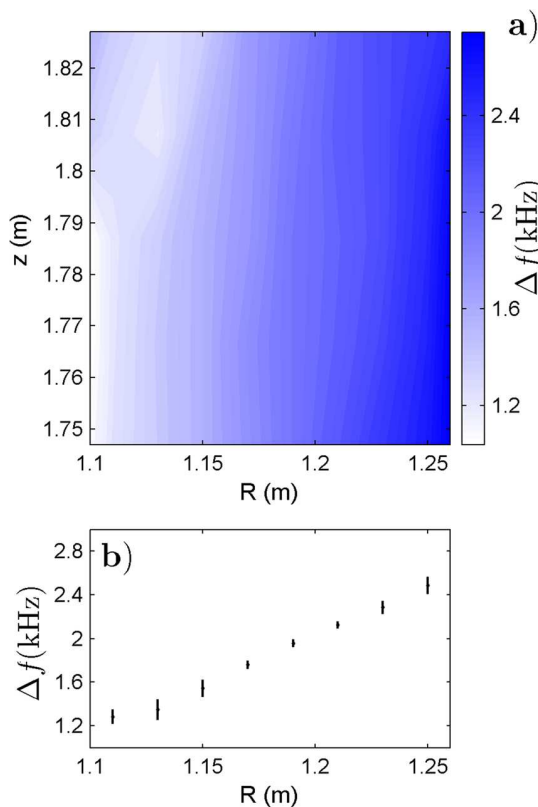
IV. INFLUENCE OF EXTERNAL BIASING ON TURBULENCE

In Texas Helimak, the turbulence power spectra can be modified by changing the radial profile of the radial electric field component. This electric field alteration can be achieved by imposing an external electric potential on some of the 16 available bias plates (see Fig. 1(a)). For the shots analyzed in this paper, bias is imposed in the four plates (two on the top and two on the bottom, on both sides of the machine, as indicated in Fig. 1(a)) placed in the interval from R = 0.86 m to R = 1.07 m, near the radial region chosen to analyze the turbulence (1.10 m < R < 1.25 m).

In Fig. 6(a), we can see the frequency width Δf of the ion saturation current power spectra obtained at different radial positions and several bias values. The obtained frequency width depends on the external bias. Namely, the fluctuation power spectra become broader for positive bias and are narrower for negative bias. Thus, application of negative bias induces frequency localized modes which will be analyzed in the next section. Moreover, in Fig. 6(a), for two specific bias values, −16 V and −20 V, we observe a strong decrease of the spectrum width, specially for radial values

FIG. 5. (a) Frequency spectrum width, Δf, for several vertical (z) and radial (R) positions. (b) Vertical average of the frequency spectrum width, Δf, for several radial positions, for a bias grounded discharge. The uncertain of each point is estimated by the standard deviation for the vertical set of values.
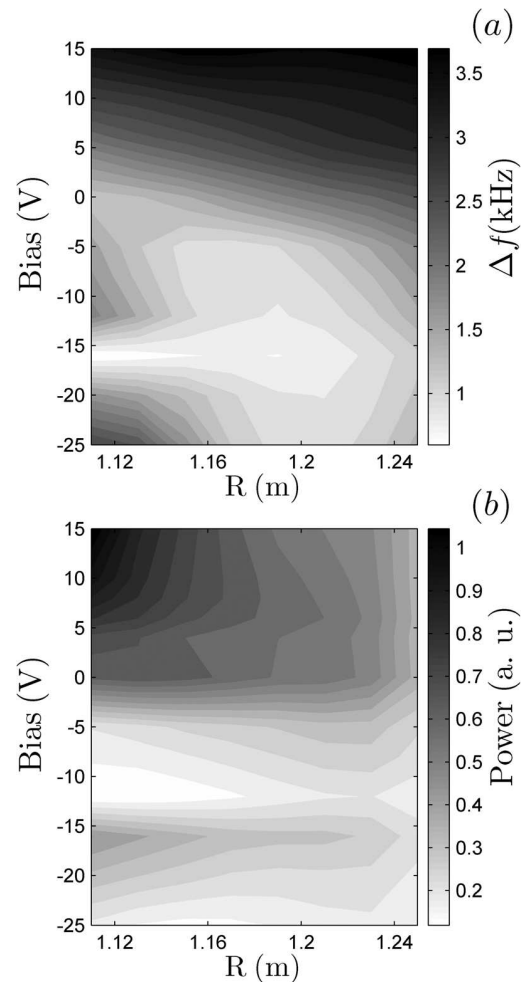

FIG. 6. Radial profiles of the spectrum width (a) and total power spectrum (b) for several bias values.

lower than 1.2 m, an indication of the presence of a macroscopic low frequency mode.

To better understand the influence of the bias on the turbulence, we present in Fig. 6(b), the total spectral power as a function of the radial positions and bias values is shown. The total spectral power was obtained integrating the power spectrum. By comparing the spectra of Figures 6(a) and 6(b), we note that high values of power and spectrum width occur for positive bias values.

Thus, varying the bias values from −25 V to 15 V, we observe the influence of the electric field on the turbulence, a continuous variation from low turbulence level and narrower spectra, for negative bias, to high turbulence level and broadband frequency spectra for positive bias.

An additional indication of two kinds of turbulence in the considered data can be obtained from the recurrence of the analyzed time series whose points are written as y_i, with $i = 1, 2, \ldots$ N. From the latter, we can make a d-dimensional embedding using vectors $X_i = (y_i, y_{i+\tau}, y_{i+2\tau}, \ldots, y_{i+(d\_1)\tau})$, where τ is a suitably chosen time delay.[27,28] The points X_i in $\mathbf{R}^d$ represent the reconstructed dynamical state of the system at a given time i. The points at times i and j of the series are said to be recurrent if $X_i \approx X_j$. A systematic way to investigate the occurrence of recurrences in a time series is by means of recurrence plots (RPs), which are two-dimensional graphical representations of the matrix whose elements are $R_{i,j} = \Theta(\varepsilon - \|X_i - X_j\|)$, i, j = 1, 2, … N, where ε is a predetermined threshold, Θ is the Heaviside unit step, $\|\ldots\|$ is the Euclidean (or another suitable) norm.[27–29] The recurrence plot is obtained by assigning a black (white) pixel to the points for which $R_{i,j} = 1(0)$. While the RPs depend on the values of the embedding dimension d and the threshold ε, the relative trend is quite stable with respect to these parameters.[27,29]

Recurrence quantification analysis consists of a series of measures obtained from a recurrence plot which can elucidate various aspects of the system behavior. For example, stationary time series give recurrence plots which are homogeneous, while for non stationary ones the recurrences are mainly concentrated close to the main diagonal. If the plot shows a cloud of points with a homogeneous yet irregular distribution, then the time series has a pronounced random nature. The formation of patterns may indicate stationary turbulent behavior, and so on.[28] Furthermore, some properties of the RPs can be quantified using the diagnostics of the so-called recurrence quantification analysis.[27,28] For instance, the *determinism* (DET) algorithm evaluates the fraction of recurrence points belonging to diagonal lines in the RPs.[27,28] Diagonal lines appear in the RPs when similar evolutions are observed in different time intervals. So, low turbulent fluctuations are expected to exhibit more recurrence points in diagonal lines than high turbulent ones (for which the recurrence points are expected to be uniformly distributed).

In Figure 7, we present the RPs obtained from the measured fluctuations for short time intervals (4 ms, corresponding to 2.000 points) with (a) bias = −30 V, (b) bias ground, and (c) bias = +15 V. For each of these RPs, we calculate the DET value.[29]

The obtained RPs are homogeneous, as expected for the analyzed stationary series. The turbulence differences can be
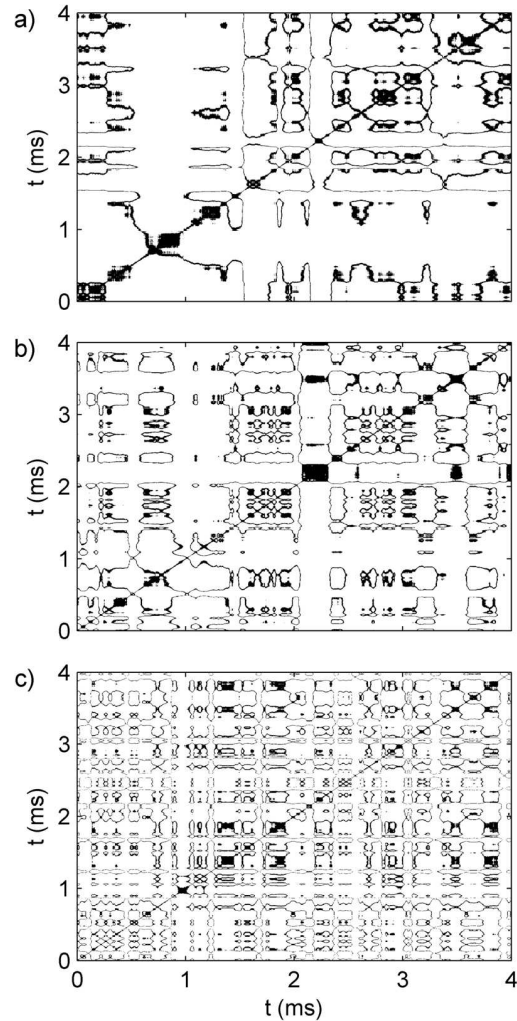

FIG. 7. Recurrence plots for shot with (a) bias = −30 V, (b) bias ground, and (c) bias = +15 V. The estimate determinism for each case is 0.93, 0.90, and 0.76, respectively. The analyzed time series of saturation current was obtained for a probe positioned on R = 1.17 m and z = 1.747 m.

identified in the three RPs of Figure 7 by their characteristic patterns, or structures, made of certain distributions of pixels. Observing these plots, we see for negative bias the size of the recurrence structures in the RPs is bigger than for positive bias. It suggested that the regularity is lower at positive bias than at negative one, which can be interpreted as an increase of the turbulence.[27] The estimated DET decreases from negative to positive bias, confirming what is observed directly by the plots: 0.93 for bias = −30 V, 0.90 for bias ground, and 0.76 for bias = +15 V.

Therefore, the dynamical analysis from the RPs confirms the results of the statistical analysis that suggests the existence of two regimes of turbulence according to the signal of the bias.

V. INTERPRETATION OF TURBULENCE ALTERATION

A. Broad frequency spectrum

The electrostatic turbulent fluctuation spectra have common properties in several plasma confinement devices. Namely, the time series of the signals are intermittent, nearly

random, the statistics of the fluctuations does not completely satisfy the assumptions of statistical homogeneity and isotropy in the plane perpendicular to the toroidal magnetic field. Usually, fluctuation PDFs and the probability distribution of time interval between successive bursts, P(τ), are used to characterize statistical properties of the electrostatic turbulence.

In Figure 8, we present PDFs of saturation current signals for three different bias values: -25 V (dashed line), ground (solid line), and $+15$ V (dotted line). These experimental curves cannot be fitted by Gaussians, as it can be recognized by comparing these distributions to the Gaussian shown in solid red thin line. The PDF of the turbulence observed for positive biasing (15 V) has a long tail, an indication of intermittent bursts. The same kind of PDF with long tail has been commonly observed in tokamak plasma edge and scrape-off layer.[30] As in tokamaks and other devices, there is a great variability in the amplitude of bursts as well as in the time interval between two successive bursts.[31,32]

To systematize the statistical analyses of the PDF shapes and evaluate the observed deviations from Gaussians, we compute the skewness and kurtosis for all discharges and indicate in Fig. 9 by axes (crosses) the results obtained with positive (negative) bias. For positive bias, the kurtosis and skewness are higher than the values $K = 3$ and $S = 0$ obtained for Gaussian distributions, indicating the presence of positive extreme events. As observed in Torpex,[31] K and S values are approximately distributed along a parabola. This deviation from a Gaussian is due to the presence of intermittent bursts, a phenomenon common to several magnetic confinement devices,[29,33] and the parabolic relationship

FIG. 9. Kurtosis versus skewness curve for bias grounded (black dots), bias > 0 (blue axes), and bias < 0 (red crosses). An estimated quadratic curve is showed to guide the interpretation.

between K and S has been observed in several kinds of plasma turbulence.[34]

Next, for data from probes at R $= 1.170$ m and a shot with bias $= +15$ V, we present in Fig. 10 the probability distribution, P(τ), of time intervals, τ, between successive bursts (considered as events with amplitude at least four times the standard deviation). In this figure, the curve is an exponential fitting. The observed exponential distribution is also observed for the inter bursts time of the intermittent fluctuation in the tokamak scrape-off layer. This distribution of τ values in the sequence of Fig. 10 indicates that the bursts appear in uncorrelated time intervals.

B. Bispectral analysis

Nonlinear mode coupling has been identified in several experiments with broadband turbulent plasmas.[35] Particularly, mode coupling has been proposed as one relevant mechanism
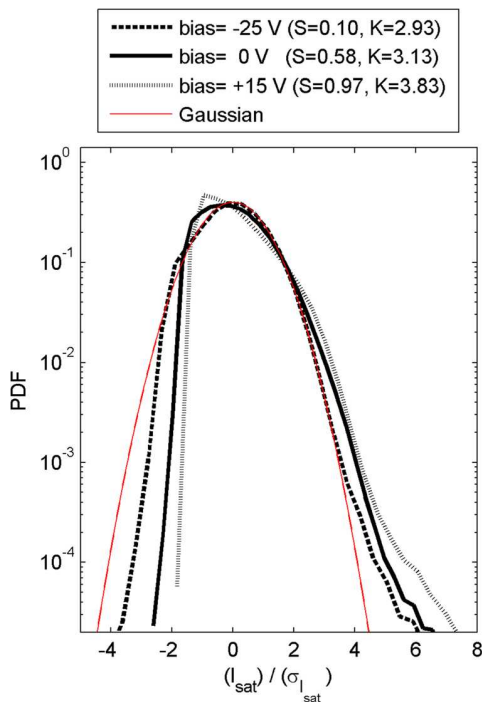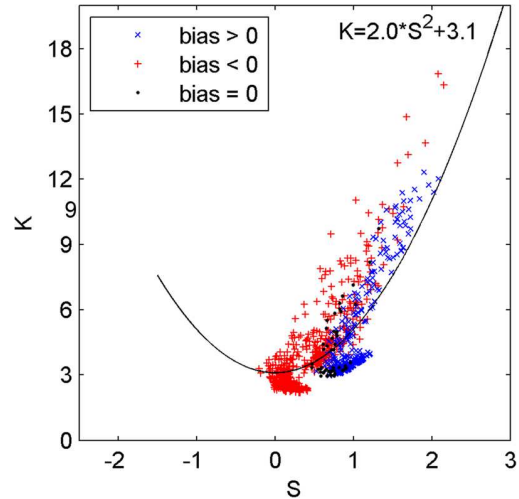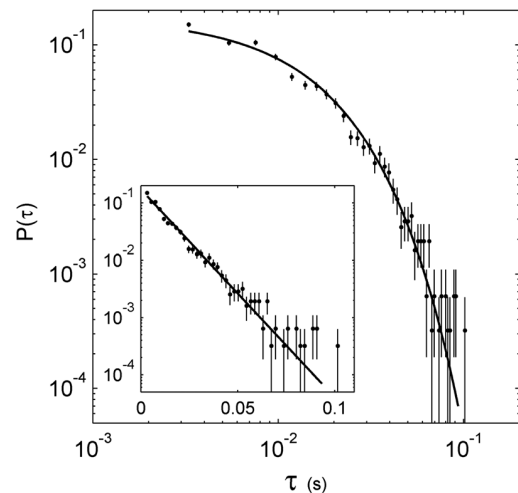

FIG. 8. PDFs of saturation current signals for three different bias values: -25 V (dashed line), ground (solid line), and $+15$ V (dotted line). A Gaussian PDF is showed for comparisons (solid red thin line).

FIG. 10. Probability distribution, P(τ), as a function of τ. Data obtained for probes at R $= 1.170$ m for a shot with bias $= +15$ V. The curve is an exponential fitting. In the inset, we show the same date with linear scale on τ axes.

for the onset of turbulence.[16] One of most fruitful procedures to identify the mode coupling and estimate its importance is the bispectral analysis.[9,36] We apply this analysis to the turbulence in Helimak to identify the bispectrum differences in discharges with positive and negative bias.

In this work, we consider the plasma turbulence spectra, like those of Fig. 3, and apply the standard procedure of bispectral analyses to identify and measure nonlinear mode couplings. The auto-bicoherency was calculated through the auto-bispectrum.[9] Taking $\phi_n(f)$ as the discrete Fourier transform of the n time signal at frequency f than the auto-bispectrum of n is

$$B(f_1, f_2) = \langle \phi_n(f_3) \phi_n^*(f_1) \phi_n^*(f_2) \rangle, \tag{7}$$

where $f_3 = f_1 + f_2$

The normalization of the auto-bispectrum gives the associated auto-bicoherency, b^2, which does not depend on the mode amplitudes

$$b^2(f_1, f_2) = \frac{|B(f_1, f_2)|^2}{\langle |\phi_n(f_1)\phi_n(f_2)|^2 \rangle \langle |\phi_n(f_3)|^2 \rangle}. \tag{8}$$

In Figure 11, we show the auto-bicoherency spectrum for one signal obtained for R = 1.21 m and z = 1.75 m and a negative bias of −8 V. In this figure, the frequencies are on the axis and the auto-bicoherency (b^2) value is in grey scale. We decide to plot only frequencies less than 1 kHz, but in the subsequent results we calculate the auto-bicoherency until f = 4 kHz. Fig. 11 auto-bicoherency spectrum shows some higher values of b^2, for example, the region where $f_1 \cong 0.20$ kHz and $f_2 \cong 0.13$ kHz, indicating the existence of coupling between modes with frequencies 0.13, 0.20, and 0.33 kHz.

In order to investigate the wave coupling dependence with the radial and vertical positions, we introduce the sum of the auto-bicoherency, $S_b = \sum_{f_1} \sum_{f_2} b^2(f_1, f_2)$, whose value reflects the amount of the wave coupling. Fig. 12(a) shows the value of the S_b as a function of the radial position. In this
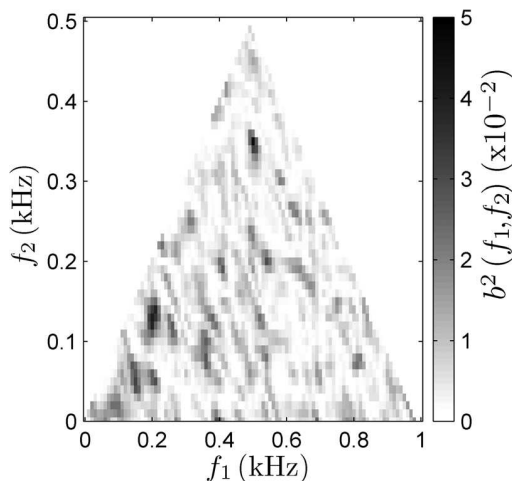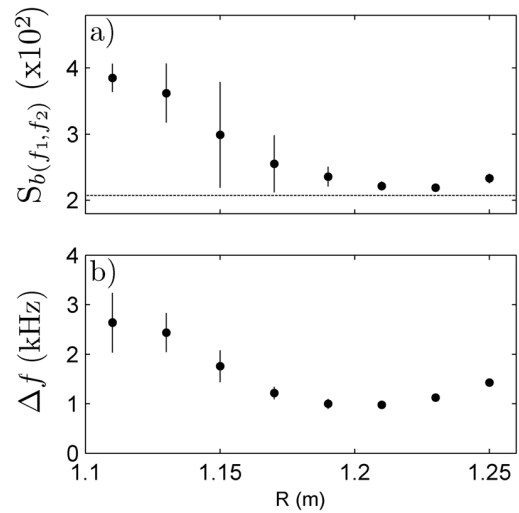

FIG. 12. (a) Sum of bicoherency, S_b, and (b) spectrum width as a function of the radial position. Discharge for a bias = −25 V. The uncertain of each point is estimated by the standard deviation for the vertical set of values. The dashed line indicates the sum of bicoherency of a random signal.

figure, we observe that the sum of the auto-bicoherency increases with the radial position, especially for R > 1.18 m.

Comparing, in Figure 12, the dependence of the S_b and the power spectrum width with the radial position presented, we note that both present similar radial profiles. This similarity could be interpreted as an evidence that, for negative bias, the spectrum width changes with the mode coupling intensity (as considered in Sec. V C).

In Figure 13, we show the auto-bicoherency spectrum for one signal obtained for R = 1.21 m and z = 1.75 m and a positive bias of +8 V. In this case, the auto-bicoherency spectrum also shows evidence of mode coupling. However, Figure 14 shows that, for discharges with positive bias, the S_b and the power spectrum width do not have similar radial profiles, suggesting that the power spectrum width is not a function of the coupling.

In Sec. V C, for discharges with negative bias, we use the dominant modes with high bicoherence values, as in
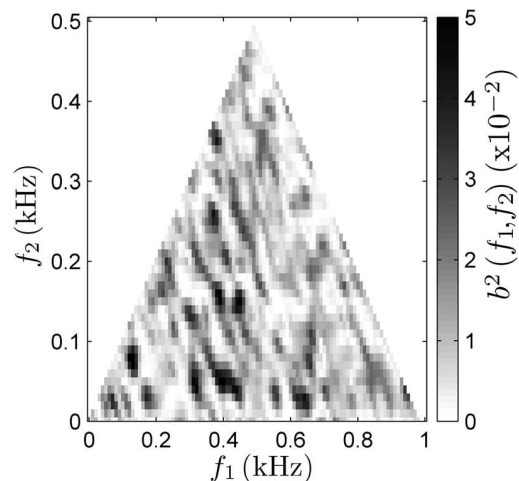

FIG. 11. Auto-bicoherency for radial position R = 1.21 m and vertical position z = 1.75 m. For the considered shot, the bias was −8 V.

FIG. 13. Auto-bicoherency for radial position R = 1.21 m and vertical position z = 1.75 m. For the considered shot, the bias was +8 V.
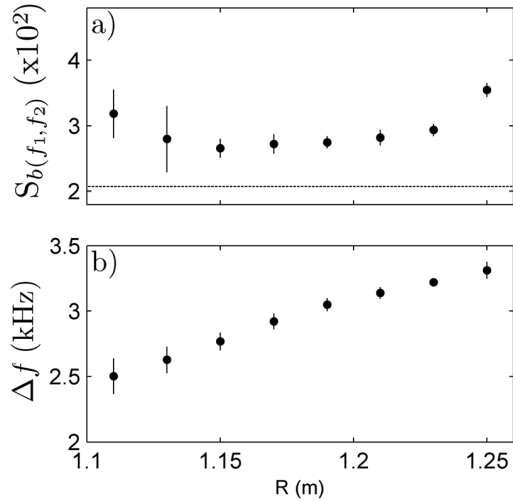
FIG. 14. (a) Sum of bicoherency, S_b, and (b) spectrum width as a function of the radial position. Discharge for a bias $= +8$ V. The uncertain of each point is estimated by the standard deviation for the vertical set of values. The dashed line indicates the sum of bicoherency of a random signal.

Figure 11, to identify the modes whose iteration with the zonal flow may explain the observed width radial dependence as the one shown in Figure 12.

C. Evidence of wave and zonal flow coupling for negative bias

Next, we use a model to describe the coupled wave propagation in Helimak discharges with negative bias. More specifically, we consider a model describing the onset of turbulence due to the coupling between the drift waves and the zonal flow. But, it is worth to mention that some interpretations of turbulence in helimaks indicate that fluctuations may be driven by drift or interchange instabilities.[17,22]

Turbulent drift fluctuations have been described by nonlinear wave equations.[3] This subject was pioneered in the field of magnetically confined plasmas by Hasegawa and his co-workers who obtained numerical solutions of Hasegawa-Mima equation for the basic nonlinear three-wave interaction.[37] In Ref. 37, the Hasegawa-Mima equation describing a nonlinear coupling of three drift waves was assumed to govern the evolution of the system to a turbulent state. It was also emphasized that such an interaction could proceed not only for the resonant case but also for the non resonant, where a significant frequency mismatch occurs. In view of this, a Generalized Charney-Hasegawa-Mima equation (GCHME) was used in Ref. 38 to describe the underlying nonlinear interaction generalized to a four-wave process. This is particularly relevant to the case where one of the interacting waves is an almost zero-frequency zonal flow, as we are considering in the present investigation.

Here, we use the GCHME to describe electrostatic drift waves in magnetically confined plasmas. We present numerical solutions for a four-wave mechanism introduced in Ref. 38, for which the energy of a pump wave, in the presence of a modulated zonal flow, is transferred to two sideband modes. Thus, in this paper, we analyze the Helimak plasma turbulence as described by the GCHME[38]

$$\left(\frac{\partial}{\partial t} + \mathbf{V}_0 \cdot \nabla + \mathbf{V}_d \cdot \nabla\right)\frac{e\tilde{\phi}}{T_e}$$
$$- \left(\frac{\partial}{\partial t} + \mathbf{V}_0 \cdot \nabla + \tilde{\mathbf{V}}_E \cdot \nabla\right)\rho_s^2 \nabla_\perp^2 \frac{e\phi}{T_e} = 0. \quad (9)$$

Here, ϕ is the total electrostatic potential given by $\phi = \bar{\phi} + \tilde{\phi}$, where $\bar{\phi}$ is the equilibrium and $\tilde{\phi}$ the fluctuation. The velocity $\mathbf{V}_0 = c\hat{\mathbf{e}}_x \times \nabla\bar{\phi}/B$ is the equilibrium flow due to the $\mathbf{E} \times \mathbf{B}$ drift and is referred to as the zonal flow, where the equilibrium magnetic field is $\mathbf{B} = B\hat{\mathbf{e}}_x$. $\mathbf{V}_d = V_d\hat{\mathbf{e}}_z$ is the diamagnetic drift with $V_d = c_s^2/(\Omega_i L_n)$, and L_n is the equilibrium density scale length, $L_n^{-1} = 1/\bar{n}|d\bar{n}/dx|$, while $\mathbf{V}_E = c\hat{\mathbf{e}}_z \times \nabla\tilde{\phi}/B$ is the fluctuating $\mathbf{E} \times \mathbf{B}$ drift and $\rho_s = c_s/\Omega_i$. The used time normalization is $t \to (\rho_s c_s/a^2)t$, where ρ_s is the ion-acoustic gyro radius, c_s is the ion sound velocity, and a is the characteristic plasma size.

Next, we simplify the problem by assuming that there is just a single, finite amplitude, monochromatic drift wave present initially, whose frequency and wave number are given by (ω_0, k_0), where $k_0 = (0, k_y, k_z)$, and

$$\omega_0 = \frac{\alpha k_z}{1 + \rho^2 k_0^2}, \quad (10)$$

where $k_0^2 = k_y^2 + k_z^2$ and $\alpha = a/L_n$.

Now, we consider the presence of a zonal flow fluctuation $(\omega, \mathbf{q})$ with wave number $\mathbf{q}$, which varies on a time scale much longer than ω_0^{-1}. The zonal flow fluctuation can then beat with the finite amplitude pump wave to generate drift wave sidebands with wave numbers, $\mathbf{k}_\pm = \mathbf{k}_0 \pm \mathbf{q} = (0, \; k_y \pm q, k_z)$. The sidebands can beat with the pump wave to reinforce the zonal flow fluctuation, thus closing the feedback loop. This is the mechanism underlying modulational instabilities which have been studied in fluids and magnetized plasmas.[38]

Introducing the amplitudes A_0, B, $a_\pm$, we have

$$\tilde{\phi}_0 = A_0(t)\exp(ik_y y + ik_z z - i\omega_0 t) + c.c. \quad (11)$$

and the sidebands

$$\tilde{\phi}_\pm = a_\pm(t)\exp\left(i(k_y \pm q)y + ik_z z - i\omega_\pm t\right) + c.c. \quad (12)$$

In this expression, the unperturbed drift wave frequencies, $\omega_\pm$, are given by

$$\omega_\pm = \frac{\alpha k_z}{1 + \rho^2 k_\pm^2}, \quad (13)$$

where $k_\pm^2 = (k_y \pm q)^2 + k_z^2$. The zonal flow perturbation is assumed to be of the following form:

$$\mathbf{V}_0 = \frac{\rho_s}{a}c_s\hat{\mathbf{e}}_z[iqB(t)\exp(iqy) + c.c.] \quad (14)$$

Substituting these waves into Eq. (9) and keeping only the terms which satisfy perfect wave number matching, we obtain the following coupled equations:

$$\frac{dA_0}{dt} = -\Omega_0 \frac{[1 + (k_+^2 - q^2)\hat{\rho}^2]}{(1 + k_0^2 \hat{\rho}^2)} a_+ B^*$$
$$+ \Omega_0 \frac{[1 + (k_-^2 - q^2)\hat{\rho}^2]}{(1 + k_0^2 \hat{\rho}^2)} a_- B, \tag{15}$$

$$\frac{da_+}{dt} + i\delta_+ a_+ = \Omega_0 \frac{[1 + (k_0^2 - q^2)\hat{\rho}^2]}{(1 + k_+^2 \hat{\rho}^2)} A_0 B, \tag{16}$$

$$\frac{da_-}{dt} + i\delta_- a_- = -\Omega_0 \frac{[1 + (k_0^2 - q^2)\hat{\rho}^2]}{(1 + k_-^2 \hat{\rho}^2)} A_0 B^*, \tag{17}$$

$$\frac{dB}{dt} = \Omega_0 \frac{(k_+^2 - k_0^2)}{q^2} a_+ A_0^* - \Omega_0 \frac{(k_-^2 - k_0^2)}{q^2} a_-^* A_0, \tag{18}$$

where $\delta_\pm = \omega_\pm - \omega_0$ and $\Omega_0 = qk_z$.

Next, we analyze numerical solutions from this model to interpret the dependence of turbulence spectrum widths with bias and radial position, observed for discharges in Texas Helimak with negative bias. To do so, we obtain from the experimental data the input parameters and integrate the system's equation. The experimental input parameters are obtained as follow. The magnetic field, B, is obtained directly using the equation B (R) = 0.077/R (T). The electronic temperature was defined as a constant and uniform $T_e \sim 13$ eV, which is consistent with the measured $I \times V$ curve of the Langmuir probes in a specific experiment. The mass of the ion (argon) is: $m_i = 6.67 \times 10^{-26}$ kg. The characteristic length of the machine is $a = 1$ m. The equilibrium density scale length, L_n, was obtained for each bias value, radial and vertical positions using the mean radial profile of the measured saturation current once we adopt

$$L_n = \frac{1/\bar{n}}{d\bar{n}/dR} \approx \frac{1/\bar{I}_{sat}}{d\bar{I}_{sat}/dR}$$

neglecting the temperature changes with the radial position. The vertical wave number, k_z, was obtained thought the S(k,f) spectrum, like the spectrum of Fig. 4, for each bias value in each vertical and radial positions. The radial wave number cannot be accurate measured, than we took it as $k_R = k_z/3$. The zonal flow wave number, q, was calculated using the bias adjusting sinusoidal curves on the sheared plasma vertical flow velocity profiles which was measured by an spectroscopic method.[8]

Integrating the system with the experimental parameters, we observe that the pump wave, the zonal flow, and the side-band waves exchange energy with each other. During this exchange, the amplitude of the waves is modulated. To interpret these experimental turbulence spectrum characteristics, the time period of this modulation can then be measured for each set of experimental input values. We conjecture that for shorter times of interaction waves, the spectrum should be broad once there is time for sideband creation and these sidebands interact with the zonal flow to create another side-bands in a recursively processes that will create many waves resulting in a broad band spectrum. To illustrate the differences in the time interaction of two different input parameters, we show in Fig. 15 the evolution of the a_+ for two different
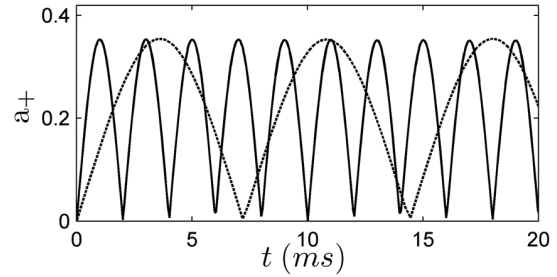

FIG. 15. The interaction time dependence on external bias potential: evolution of amplitude of the sideband (a_+) for two different radial positions: R = 1.11 m (dashed line) and R = 1.21 m (solid line), both for the same bias value, −25 V z = 1.747 m.

radial positions: R = 1.11 m (a) and R = 1.21 m (b), both for the same bias value, −25 V, and vertical position z = 1.747 m.

In order to interpret the spectrum width dependence with the radial position and the external bias values, in the framework of the considered wave coupling, we theoretically estimate the mean value of the wave interaction time, for several radial positions and negative bias values. This dependence is shown in Fig. 16, where we observe that the
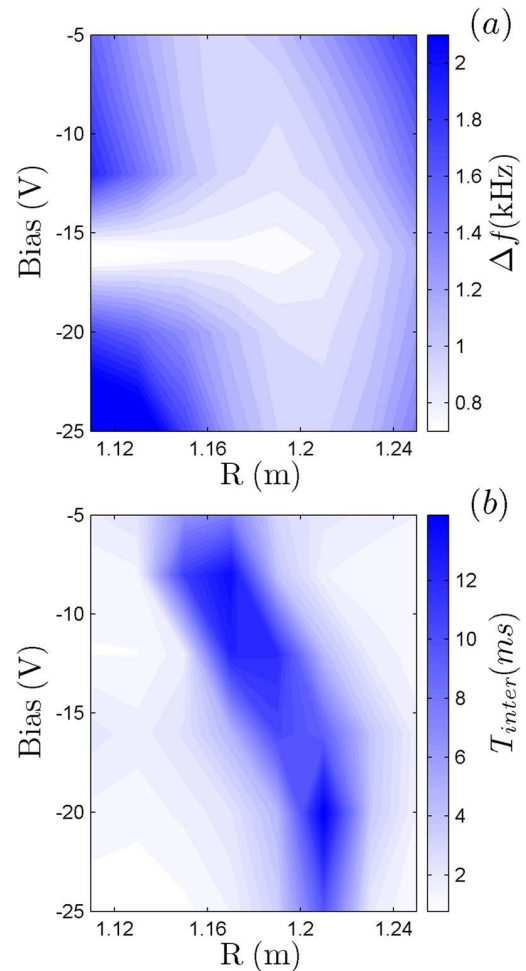

FIG. 16. Interaction time (a) and power spectrum width (b) for several bias voltages and the radial positions.

interaction time present a region of high values (from $R \sim 1.16$ m and bias ~ -8 V to $R \sim 1.21$ m and bias ~ -22 V) similar to the region where the spectrum width present small values. We note that the model estimated interaction time does not taken into account the low frequency mode observed for bias ≈ -16 V and $R < 1.2$ m.

In the analyzed Helimak discharges, with negative bias, the spectrum widths depend on the radial coordinate (see Figure 12). The results obtained in this section indicate that the experimentally observed spectrum width increases where the coupling interaction time, estimated from GCHME solutions, decreases. Consequently, in the regions with long interaction time, the wave coupling with the zonal flow recursively generates a sequence of daughter waves during the wave propagation in Helimak.

VI. CONCLUSIONS

In Texas Helimak, the turbulence has been investigated in a sheared flow one dimensional equilibrium plasma. As the plasma is cold and rarified, a large set of Langmuir probes can be used to measure the fluctuations inside the plasma. Moreover, the ion flow velocity profile is spectroscopically measured. The turbulence level has been reduced by controlling the radial electric field using a set of metal plates at the top and bottom inside the vessel. Thus, investigations performed in Texas Helimak could be of considerable value to elucidate the influence of the electric field and zonal flow radial profiles on plasma turbulence.

In this article, we analyzed the plasma turbulence in Texas Helimak, in a roughly uniform gradient region, in the discharges with biased electric fields, and identify a continuous variation from low turbulence level, for negative bias, to high turbulence level for positive bias. By applying spectral, statistical, and recurrence analyses, we identified two different kinds of perturbed turbulence. Overall, for positive biasing, turbulence shows enhanced broadband spectra and non Gaussian PDF with extreme events. On the other hand, when applying a negative bias, turbulence level is reduced. In this case, the spectral width increases with the wave coupling. Moreover, large frequency widths occur for short growth rate of the sidebands associated to the recursively coupling between the drift waves and the zonal flow.

In conclusion, our analysis of Texas Helimak data reveals new features that may contribute to better understand the influence of the electric field radial profile on the turbulence observed in magnetically confined plasmas.

[1]C. Hidalgo, Astrophys. Space Sci. **292**, 681(2004).
[2]R. D. Hazeltine and S. C. Prager, Phys. Today **55**(7), 30 (2002).

[3]W. Horton, Rev. Mod. Phys. **71**, 735 (1999).
[4]X. Garbet, Plasma Phys. Controlled Fusion **43**, A251 (2001).
[5]C. Hidalgo, C. Alejaldre, A. Alonso, J. Alonso, L. Almoguera, F. de Aragón, E. Ascasíbar, A. Baciero, R. Balbín, E. Blanco, J. Botija, B. Brañas, E. Calderón, A. Cappa, J. A. Carmona, R. Carrasco, F. Castejón, J. R. Cepero, A. A. Chmyga, J. Doncel, N. B. Dreval, S. Eguilior, L. Eliseev, T. Estrada, J. A. Ferreira, A. Fernández, J. M. Fontdecaba, C. Fuentes, A. García, I. García-Cortés, B. Gonçalves, J. Guasp, J. Herranz, A. Hidalgo, R. Jiménez, J. A. Jiménez, D. Jiménez-Rey, I. Kirpitchev, S. M. Khrebtov, A. D. Komarov, A. S. Kozachok, L. Krupnik, F. Lapayese, M. Liniers, D. López-Bruna, A. López-Fraguas, J. López-Rázola, A. López-Sánchez, E. de la Luna, G. Marcon, R. Martán, K. J. McCarthy, F. Medina, M. Medrano, A. V. Melnikov, P. Méndez, B. van Milligen, I. S. Nedzelskiy, M. Ochando, O. Orozco, J. L. de Pablos, L. Pacios, I. Pastor, M. A. Pedrosa, A. de la Peña, A. Pereira, A. Petrov, S. Petrov, A. Portas, D. Rapisarda, L. Rodríguez-Rodrigo, E. Rodríguez-Solano, J. Romero, A. Salas, E. Sánchez, J. Sánchez, M. Sánchez, K. Sarksian, C. Silva, S. Schchepetov, N. Skvortsova, F. Tabarés, D. Tafalla, A. Tolkachev,V. Tribaldos, I. Vargas, J. Vega, G. Wolfers, and B. Zurro, Nucl. Fusion **45**, S266 (2005).
[6]G. Van Oost, J. Adámek, V. Antoni, P. Balan, J. A. Boedo, P. Devynck, I. Duran, L. Eliseev, J. P. Gunn, M. Hron, C. Ionita, S. Jachmich, G. S. Kirnev, E. Martines, A. Melnikov, R. Schrittwieser, C. Silva, J. Stöckel, M. Tendler, C. Varandas, M. Van Schoor, V. Vershkov, and R. R. Weynants, Plasma Phys. Controlled Fusion **45**, 621 (2003).
[7]I. C. Nascimento, Y. K. Kuznetsov, J. H. F. Severo, A. M. M. Fonseca, A. Elfimov, V. Bellintani, M. Machida, M. V. A. P. Heller, R. M. O. Galvão, E. K. Sanada, and J. I. Elizondo, Nucl. Fusion **45**, 796 (2005).
[8]K. W. Gentle, K. Liao, K. Lee, and W. L. Rowan, Plasma Sci. Technol. **12**, 391 (2010).
[9]Ch. P. Ritz, E. J. Power, T. L. Rhodes, R. D. Bengtson, K. W. Gentle, H. Lin, P. E. Phillips, A. J. Wootton, D. L. Brower, N. C. Luhmann Jr., W. A. Peebles, P. M. Schoch, and R. L. Hickok. Rev. Sci. Instrum. **59**, 1739 (1988).
[10]J. S. Kim, R. J. Fonck, R. D. Durst, E. Fernandez, P. W. Terry, S. F. Paul, and M. C. Zarnstortt, Phys. Rev. Lett. **79**, 841 (1997).
[11]P. W. Terry, Rev. Mod. Phys. **72**, 109 (2000).
[12]B. Li, B. N. Rogers, P. Ricci, K. W. Gentle, and A. Bhattacharjee, Phys. Rev. E **83**, 056406 (2011).
[13]U. Kauschke, G. Oelerich-Hill, and A. Piel, Phys. Fluids B **2**, 38 (1990).
[14]C. Riccardi, D. Xuantong, M. Salierno, L. Gamberale, and M. Fontanesi, Phys. Plasmas **4**, 3749 (1997).
[15]F. J. Øynes, O. M. Olsen, H. L. Pécseli, Å. Fredriksen, and K. Rypdal, Phys. Rev. E **57**, 2242 (1998).
[16]A. A. Ferreira, M. V. A. P. Heller, and I. L. Caldas, Phys. Plasmas **7**, 3567 (2000).
[17]W. Horton, J. C. Pèrez, T. Carter, and R. Bengtson, Phys. Plasmas **12**, 022303 (2005).
[18]W. Gekelman, H. Pfister, Z. Lucky, J. Bamber, D. Leneman, and J. Maggs., Rev. Sci. Instrum. **62**, 2875 (1991).
[19]T. A. Carter and J. E. Maggs, Phys. Plasmas **16**, 012304 (2009).
[20]K. W. Gentle and Huang He, Plasma Sci. Technol. **10**, 284 (2008).
[21]K. Rypdal and S. Ratynskaia, Phys. Rev. Lett. **94**, 225002 (2005).
[22]P. Ricci, B. N. Rogers, and S. Brunner, Phys. Rev. Lett. **100**, 225002 (2008).
[23]S. H. Miller, A. Fasoli, B. Labit, M. McGrath, O. Pisaturo, G. Plyushchev, M. Podestà, and F. M. Poli, Phys. Plasmas **12**, 090906 (2005).
[24]S. Luckhardt, "The Helimak: A one dimensional toroidal plasma system," Technical Report No. UCSD-ENG-069 (University of California, San Diego, 1999), see http://orion.ph.utexas.edu/~starpower.
[25]J. C. Perez, W. Horton, K. W. Gentle, W. L. Rowan, K. Lee, and R. B. Dahlburg, Phys. Plasmas **13**, 032101 (2006).
[26]D. Toufen, Z. Guimarães Filho, I. L. Caldas, F. A. Marcus, and K. Gentle, Phys. Plasmas **19**, 012307 (2012).
[27]Z. O. Guimarães-Filho, I. L. Caldas, R. L. Viana, J. Kurths, I. C. Nascimento, and Yu. K. Kuznetsov, Phys. Lett. A **372**, 1088 (2008).
[28]N. Marwan, M. C. Romano, M. Thiel, and J. Kurths Phys. Rep. **438**, 237 (2007).
[29]Z. O. Guimarães-Filho, I. L. Caldas, R. L. Viana, I. C. Nascimento, Yu. K. Kuznetsov, and J. Kurths, Phys. Plasmas **17**, 012303 (2010).
[30]P. Devynck, G. Antar, G. Wang, X. Garbet, J. Gunn, and J. Y. Pascal, Plasma Phys. Controlled Fusion **42**, 327 (2000).

[31]B. Labit, I. Furno, A. Fasoli, A. Diallo, S. H. Müller, G. Plyushchev, M. Podestà, and F. M. Poli, Phys. Rev. Lett. **98**, 255002 (2007).

[32]G. Y. Antar, S. I. Krasheninnikov, P. Devynck, R. P. Doerner, E. M. Hollmann, J. A. Boedo, S. C. Luckhardt, and R. W. Conn, Phys. Rev. Lett. **87**, 065001 (2001).

[33]G. Y. Antar, Phys. Rev. Lett. **91**, 055002 (2003).

[34]I. Sandberg, S. Benkadda, X. Garbet, G. Ropokis, K. Hizanidis, and D. del-Castillo-Negrete, Phys. Rev. Lett. **103**, 165001 (2009).

[35]A. E. White, S. J. Zweben, M. J. Burin, T. A. Carter, T. S. Hahm, J. A. Krommes, and R. J. Maqueda, Phys. Plasmas **13**, 072301 (2006).

[36]B. Ph. van Milligen, T. Kalhoff, M. A. Pedrosa, and C. Hidalgo, Nucl. Fusion **48**, 115003 (2008).

[37]A. Hasegawa, C. G. McClennan, and Y. Kodama, Phys. Fluids **22**, 2122 (1979).

[38]C. N. Lashmore-Davies, A. Thyagaraja, and D. R. McCarthy, Phys. Plasmas **12**, 122304 (2005).